Niche Partitioning Among *Prochlorococcus* Ecotypes Along Ocean-Scale Environmental Gradients

Zackary I. Johnson,[1,2]* Erik R. Zinser,[1,3]* Allison Coe,[1] Nathan P. McNulty,[1] E. Malcolm S. Woodward,[4] Sallie W. Chisholm[1]†

Prochlorococcus is the numerically dominant phytoplankter in the oligotrophic oceans, accounting for up to half of the photosynthetic biomass and production in some regions. Here, we describe how the abundance of six known ecotypes, which have small subunit ribosomal RNA sequences that differ by less than 3%, changed along local and basin-wide environmental gradients in the Atlantic Ocean. Temperature was significantly correlated with shifts in ecotype abundance, and laboratory experiments confirmed different temperature optima and tolerance ranges for cultured strains. Light, nutrients, and competitor abundances also appeared to play a role in shaping different distributions.

The marine cyanobacterium genus *Prochlorococcus* (*1*) is the numerically dominant phytoplankter in tropical and subtropical oceans (*2*–*5*). It is distributed throughout the illuminated surface waters from about 40°N to 40°S, can be found as deep as 200 m, and sometimes reaches abundances greater than 10^5 cells per ml (*2*). *Prochlorococcus* can account for 21 to 43% of the photosynthetic biomass in oligotrophic oceans and 13 to 48% of the net primary production (*4*–*6*). As such, its abundance and dynamics have a substantial impact on open ocean ecosystems and global biochemical cycles.

In the tropical and subtropical Atlantic Ocean, *Prochlorococcus* maintains its numerical dominance throughout most of the year, despite 10-fold changes in depth-integrated abundance (*3*, *6*). It reaches its maximum (*6*, *7*) when surface waters are highly stratified and devoid of major nutrients (*8*) and its minimum during deep winter mixing when blooms of *Synechococcus* and larger eukaryotic phytoplankton occur (*3*, *6*, *7*). *Prochlorococcus* abundance falls off sharply at higher latitudes, suggesting that temperature, or some related variable, is an important factor in shaping its global distributions (*2*).

Phylogenetic trees constructed with several marker genes, including small subunit (SSU) ribosomal RNA (rRNA), the rRNA internal transcribed spacer (ITS) regions, *psbB*, *petB/D*, and *rpoC1*, as well as whole-genome analyses, show that flow-cytometrically defined (*9*) *Prochlorococcus* is a genetically diverse group with several distinct clades, which have SSU rRNA gene sequences that differ by less than 3% (*10*–*14*). Cultured strains belonging to different clades have different pigmentation, maximum growth rates, metal tolerances, nutrient utilization, and photophysiological characteristics, and thus these clades have been called ecotypes (*15*–*17*). The ecotypes have recently been named after type strains with the prefix "e" (*18*, *19*). Cells belonging to different ecotypes are distributed differently along environmental gradients. For example, high light–adapted ecotypes [sensu (*12*)] such as eMIT9312 and eMED4 are more abundant near the surface than low light–adapted ecotypes such as eSS120, eMIT9313, eNATL2A, and eMIT9211 (*18*–*20*), which are typically most abundant in the deeper waters.

To better understand the drivers of ecotypic differentiation between *Prochlorococcus* clades, we measured, by using quantitative polymerase chain reaction (qPCR), the abundance of cells belonging to the six known ecotypes (fig. S1) as a function of depth along a meridional transect in the Atlantic Ocean (AMT) (*21*) (Fig. 1A). We then analyzed the distribution and abundance of ecotypes in the context of relevant environmental variables and the physiological properties of type strains.

The AMT transect covered a broad range of biogeochemical provinces (*22*), with surface temperatures ranging from 5°C to 29°C (Fig. 1A). The availability of major phytoplankton nutrients, including nitrate, nitrite, ammonium, phosphate, and silicate, also varied, reaching maxima in the south, near the coastal Canary Current upwelling system, and around the equatorial upwelling region (Fig. 1D and fig. S2). For all locations, nitrate, phosphate, and silicate concentrations were correlated (r^2 = 0.9), following near Redfield ratios (15 N/1 P/1 to 10 Si), whereas nitrite and ammonium were localized to specific regions and depths and did not follow strict relationships with other nutrients (figs. S2 and S3). Consistent with these nutrient patterns, surface chlorophyll fluorescence, an indicator of autotrophic biomass, was elevated at high latitudes and in the Canary Current upwelling system but remained low in the severely nutrient-limited subtropical gyres (Fig. 1A).

Ecotype distributions. The depth distributions of *Prochlorococcus* ecotypes at three stations representing different biogeochemical provinces revealed distinctly different patterns (Fig. 1B). Although total *Prochlorococcus* abundance (which was measured independently by using flow cytometry) was maximal at the surface and decreased with depth at each station, the ecotypes comprising this total had different distributions. In well-stratified waters (1°N and 25°N in Fig. 1B), ecotype depth distributions had a stacked nature typical of these environmental conditions (*18*, *19*). The high light–adapted clades eMIT9312 or eMED4 dominated near the surface (~0 to 50 m), and low light–adapted eNATL2A increased in abundance at middepths (~75 m), followed by eMIT9313, another low-light clade. Closer examination of the patterns at these two stations, however, revealed subtle differences that suggest that light adaptation was not the only variable shaping distributions. At 1°N, for example, eNATL2A and eMED4, low and high light–adapted clades, respectively, were roughly equal in abundance at the surface, whereas at 25°N eNATL2A was orders of magnitude less abundant than eMED4 near the surface. At high latitudes such as 48°N (Fig. 1B), one of the high light–adapted clades, eMED4, outnumbered the other, eMIT9312, by orders of magnitude in surface waters. Furthermore, the low light–adapted clade eMIT9313, which displayed deep subsurface maxima (~100 m) at low and midlatitudes, was so reduced in numbers at high latitudes that it was near the limit of detection. As has been previously reported (*18*, *19*), two of the clades, eMIT9211 and eSS120, were present at low concentrations (<50 cells per ml) in all samples and thus were not included in this part of our analysis (fig. S4).

Similar shifts in ecotype dominance were also revealed by ecotype depth-integrated abundances along the entire transect (Fig. 1C), despite relatively constant (~1×10^7 to 2×10^7 cells per mm^2) total *Prochlorococcus* concentrations. Overall, high light–adapted eMIT9312 was the dominant ecotype, exceeding the abundance of other ecotypes by two orders of magnitude between 15°N and 15°S. Low light–adapted ecotypes eNATL2A and eMIT9313 had roughly equal abundance in this part of the transect, and high light–adapted

[1]Department of Civil and Environmental Engineering, Massachusetts Institute of Technology, 15 Vassar Street 48-419, Cambridge, MA 02139, USA. [2]Department of Oceanography, University of Hawaii, 1000 Pope Road MSB614, Honolulu, HI 96822, USA. [3]Department of Microbiology, University of Tennessee, M409 WLS, Knoxville, TN 37996, USA. [4]Plymouth Marine Laboratory, Prospect Place, The Hoe, Plymouth PL1 3DH, UK.

*These authors contributed equally to this work.
†To whom correspondence should be addressed. E-mail: chisholm@mit.edu

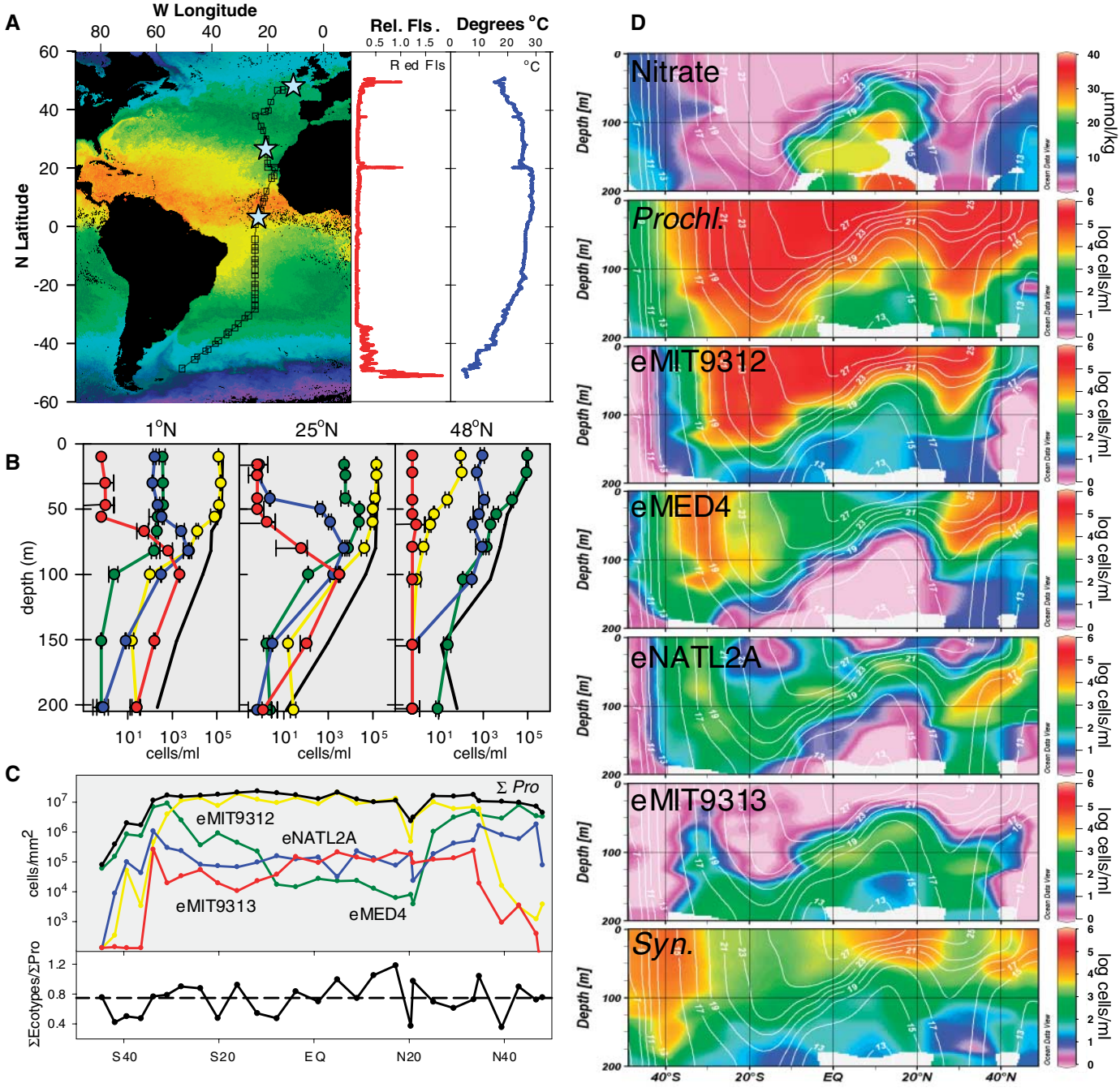

Fig. 1. (**A**) False-color image of sea surface temperature during the Atlantic Ocean meridional transect cruise (AMT13) from September to October 2003, overlaid with cruise track and sampled stations (boxes). Reds are warm temperatures; blues are cold temperatures. (Right) In situ measured surface red fluorescence (relative) (Rel. Fls), indicative of chlorophyll concentrations and temperature. The cruise track goes through the coastal Canary Current upwelling feature around 20°N. (**B**) Depth profiles of the abundance of four dominant *Prochlorococcus* ecotypes (red, eMIT9313; blue, eNATL2A; green, eMED4; and yellow, eMIT9312) and total *Prochlorococcus* cell concentrations (solid black) from three representative stations [stars in (A)]. The 1°N station is typical of equatorial region stations, 25°N is typical of stratified subtropical stations, and 48°N is typical of high-latitude (not polar) stations. Note that the abundance scale is logarithmic. Error bars indicate one standard deviation of the mean. (**C**) (Top) Depth-integrated (0 to 200 m) ecotype abundance and total *Prochlorococcus* abundance over the transect. (Bottom) Meridional distribution of the ratio of the summed ecotype abundances measured by qPCR and total *Prochlorococcus* abundance determined by flow cytometry. (**D**) Cross sections along the transect (upper 200 m) of nitrate concentration (µmol kg^{-1}); total *Prochlorococcus* (log cells per ml); dominant ecotype clade abundances (log cells per ml) for eMIT9312, eMED4, eNATL2A, and eMIT9313; and *Synechococcus* (log cells per ml). Temperature contour lines are shown in white.

eMED4 was the least abundant. By contrast, in cooler, well-mixed, nutrient-rich, high-latitude waters where eMED4 achieved numerical dominance, eMIT9313 disappeared, and eNATL2A achieved the second highest abundance. eMIT9312, the most abundant clade in the tropical and subtropical oceans, was below the detection limit at latitudes above 42°S. Our qPCR primers, designed from sequences of cultured isolates, captured on average ~75% (range from 35 to 118%) of the total *Prochlorococcus* population counted by using flow cytometry (Fig. 1C),

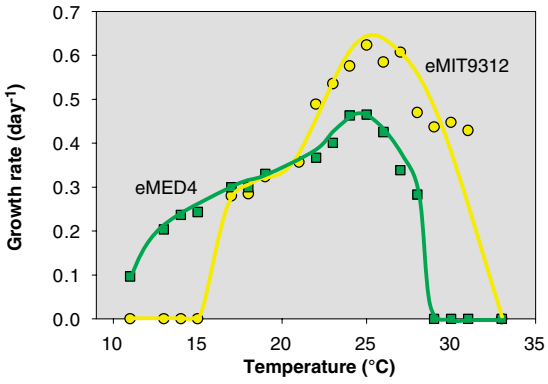

Fig. 2. Maximum growth rate as a function of temperature derived from the analysis of cultured strains belonging to the eMIT9312 clade (yellow) and the eMED4 clade (green), the two dominant near-surface ecotypes. (Specific strain data are shown in fig. S5.)

indicating that there are likely additional members not quantified in this study. However, there was no pattern to the residuals, suggesting that our observations were not greatly affected by culture bias (*23*).

Environmental factors and ecotype abundance. By using nitrate concentration to represent a suite of covarying nutrients (figs. S2 and S3), depth as related to light intensity, and plotting temperature contours on a slice through the upper 200 m along the transect, we visualized how ecotype abundances map on to environmental gradients (Fig. 1D). As expected, total *Prochlorococcus* cell concentrations were typically highest at or near the surface and decreased with depth. They were also highest in warm waters, which here are defined as waters above the 17°C isotherm, except below 150 m, where populations were likely limited by light availability. Lastly, total *Prochlorococcus* abundances were highest where nutrients were lowest, consistent with findings in other tropical and subtropical oligotrophic regions (*4*, *6*, *7*, *24*).

These patterns of total *Prochlorococcus* abundance emerge from the distributions of ecotypes, which display more complex behavior when viewed individually. For example, the relative abundances of the high light–adapted ecotypes (eMIT9312 and eMED4) depended on latitude and closely followed nutrient and temperature contours (Fig. 1D). eMIT9312 dominated at low and midlatitudes but was progressively replaced by eMED4 at latitudes above 30°. Thus, these two ecotypes, which differ in their SSU rRNA sequences by less than 1% (*12*), had overlapping but distinct niches in the Atlantic Ocean and comprised the majority (93%) of the *Prochlorococcus* cells over the transect.

Ecotypes eMIT9313 and eNATL2A had more restricted distributions. eNATL2A was most prevalent along the trailing edge of the eMIT9312 abundance contour and was most abundant in waters between the 15°C and 23°C isotherms. This distribution started at the surface waters of 45°N, meandered in the water column in mid- and low latitudes, and reached higher abundances again at the surface waters near 30°S. eNATL2A only reached high concentrations in deeper waters, where eMIT9312 and eMED4 numbers were reduced. Similarly, eMIT9313's distribution was more patchy and localized to specific latitudes or depths, closely following the vertical gradients of eMIT9312 and eMED4, and was maximal where total *Prochlorococcus* abundance decreased the most sharply with depth. Thus, although eNATL2A and eMIT9313 were minor contributors to overall *Prochlorococcus* numbers in the Atlantic Ocean, they dominated at certain depths and latitudes.

Regression analysis. The geographic patterns of *Prochlorococcus* and its ecotypes suggest causal relationships with environmental variables (Fig. 1D). We used stepwise regression analyses to investigate relationships with temperature, light, nitrate, nitrite, ammonia, phosphate, and *Synechococcus* (a potential competitor) (table S1). As has been observed previously (*25*), a significant fraction (26%, $P < 0.01$) of the variability in the total *Prochlorococcus* population could be explained by temperature, which was largely driven by significant correlations between the numerically dominant ecotype, eMIT9312, and temperature (56%, $P < 0.01$). By using laboratory isolates belonging to the two dominant (and high light–adapted) ecotypes, we found that, although both had similar temperature optima for growth, members of eMIT9312 grew faster at this temperature (25°C) and could tolerate warmer temperatures than eMED4. The latter could grow at temperatures below 15°C, however, whereas eMIT9312 could not (Fig. 2 and fig. S5), thus confirming the importance of temperature in defining ecotype niche space.

Prochlorococcus ecotype abundances are related to other variables as well. For example, eMED4 was correlated (9%, $P < 0.01$) with light, which is consistent with its adaptations to high light (*16*). Nutrient relationships were complex (often being anticorrelated with ecotypes) (table S1) and were generally not consistent with the ability of strains to use nutrient sources (*17*, *26*), suggesting that colinear variables not measured here were responsible for these relationships. Integrated abundances of *Synechococcus* (Fig. 1D), which unlike *Prochlorococcus* can use nitrate (*17*), were also inversely related to *Prochlorococcus* (fig. S6). This relationship has been found before for seasonal cycles in the Atlantic Ocean (*3*, *6*) and implies that at high nutrient levels *Synechococcus* and larger phytoplankton may exclude *Prochlorococcus*. But this relationship with *Synechococcus* was complex: eMIT9313 was anticorrelated (22% of the variability), eMED4 (18%) and eMIT9312 (10%) were correlated, and the abundance of eNATL2A was uncorrelated.

The stepwise regressions, which had varying degrees of success in explaining the overall abundance patterns, also demonstrated that there were additional factors that were important in determining *Prochlorococcus* ecotype abundance. This complexity is likely governed by differential susceptibility to viruses (*27*) and protozoan grazers (*28*) as well as other factors, such as metal tolerances (*15*).

The relationships we have established here represent only a broad-brush assessment, to be refined as we learn more about *Prochlorococcus* microdiversity. By design, multiple ribotypes (based on ITS sequences) are represented in the ecotype populations that are enumerated by our qPCR primers (*18*), and it is likely that each of these is a physiological and genomic variant. This prompts the question: If one designed primers to enumerate ribotypes within the ecotype clusters, what would their distributions look like along these gradients? Would they be more similar to each other than to those belonging to other clades? Furthermore, although the four dominant ecotypes account for the majority of the total *Prochlorococcus* population, our analyses (Fig. 1), as well as evidence from clone libraries (*18*) and Sargasso Sea shotgun sequencing (*29*), reveal the existence of additional genotypes that do not group with any of the six defined genetic clades and thus would not be captured by our approach. These additional clades likely account for the difference between the total *Prochlorococcus* population measured by flow cytometry and the summed clades measured by qPCR (Fig. 1C), particularly in the deeper waters (Fig. 1B).

References and Notes

1. S. W. Chisholm *et al.*, *Nature* **334**, 340 (1988).
2. F. Partensky *et al.*, *Microbiol. Mol. Biol. Rev.* **63**, 106 (1999).
3. R. J. Olson *et al.*, *Deep-Sea Res. Part I Oceanogr. Res. Pap.* **37**, 1033 (1990).
4. L. Campbell *et al.*, *Deep-Sea Res. Part I Oceanogr. Res. Pap.* **44**, 167 (1997).
5. D. Vaulot, D. Marie, R. J. Olson, S. W. Chisholm, *Science* **268**, 1480 (1995).
6. M. D. DuRand *et al.*, *Deep-Sea Res. Part II Top. Stud. Oceanogr.* **48**, 1983 (2001).
7. M. V. Zubkov *et al.*, *Prog. Oceanogr.* **45**, 369 (2000).
8. Z. Johnson, P. Howd, *Deep-Sea Res. Part I Oceanogr. Res. Pap.* **47**, 1485 (2000).
9. L. R. Moore *et al.*, *Nature* **393**, 464 (1998).
10. E. Urbach *et al.*, *J. Mol. Evol.* **46**, 188 (1998).
11. E. Urbach, S. W. Chisholm, *Limnol. Oceanogr.* **43**, 1615 (1998).
12. G. Rocap *et al.*, *Appl. Environ. Microbiol.* **68**, 1180 (2002).
13. G. Rocap *et al.*, *Nature* **424**, 1042 (2003).
14. B. Palenik, R. Haselkorn, *Nature* **355**, 265 (1992).
15. E. L. Mann *et al.*, *Limnol. Oceanogr.* **47**, 976 (2002).

16. L. R. Moore, S. W. Chisholm, *Limnol. Oceanogr.* **44**, 628 (1999).
17. L. R. Moore *et al.*, *Limnol. Oceanogr.* **47**, 989 (2002).
18. E. Zinser *et al.*, *Appl. Environ. Microbiol.* **72**, 723 (2006).
19. N. Ahlgren *et al.*, *Environ. Microbiol.* **8**, 441 (2006).
20. N. J. West, D. J. Scanlan, *Appl. Environ. Microbiol.* **65**, 2585 (1999).
21. J. Aiken *et al.*, *Prog. Oceanogr.* **45**, 257 (2000).
22. S. B. Hooker *et al.*, *Prog. Oceanogr.* **45**, 313 (2000).
23. M. S. Rappe, S. J. Giovannoni, *Annu. Rev. Microbiol.* **57**, 369 (2003).
24. L. Campbell *et al.*, *Deep-Sea Res. Part II Top. Stud. Oceanogr.* **45**, 2301 (1998).
25. K. K. Cavender-Bares *et al.*, *Deep-Sea Res. Part I Oceanogr. Res. Pap.* **48**, 2373 (2001).
26. L. R. Moore *et al.*, *Aquat. Microb. Ecol.* **39**, 257 (2005).
27. M. B. Sullivan *et al.*, *Nature* **424**, 1047 (2003).
28. B. C. Monger *et al.*, *Limnol. Oceanogr.* **44**, 1917 (1999).
29. J. C. Venter *et al.*, *Science* **304**, 66 (2004).
30. The authors acknowledge C. Robinson and the captain and crew of Royal Research Ship *James Clark Ross* for our participation in the AMT cruise and D. Veneziano for guidance with the statistical analysis. This work was funded in part by the Gordon and Betty Moore Foundation, the Seaver Foundation, NSF Biological Oceanography Division (to S.W.C.), and U.S. Department of Energy (to S.W.C.), NOAA and the University of Hawaii (to Z.I.J.), and NSF and the University of Tennessee (to E.R.Z.). It was also supported by the UK Natural Environment Research Council through the AMT consortium (NER/O/S/2001/00680). This is School of Ocean and Earth Science and Technology contribution no. 6686 and AMT contribution no. 107.

Supporting Online Material
www.sciencemag.org/cgi/content/full/311/5768/1737/DC1
Materials and Methods
Figs. S1 to S6

27 July 2005; accepted 11 January 2006
10.1126/science.1118052

REPORTS

General Strategies for Nanoparticle Dispersion

Michael E. Mackay,[1,2]* Anish Tuteja,[1] Phillip M. Duxbury,[2] Craig J. Hawker,[3,4] Brooke Van Horn,[4] Zhibin Guan,[5] Guanghui Chen,[5] R. S. Krishnan[1]

Traditionally the dispersion of particles in polymeric materials has proven difficult and frequently results in phase separation and agglomeration. We show that thermodynamically stable dispersion of nanoparticles into a polymeric liquid is enhanced for systems where the radius of gyration of the linear polymer is greater than the radius of the nanoparticle. Dispersed nanoparticles swell the linear polymer chains, resulting in a polymer radius of gyration that grows with the nanoparticle volume fraction. It is proposed that this entropically unfavorable process is offset by an enthalpy gain due to an increase in molecular contacts at dispersed nanoparticle surfaces as compared with the surfaces of phase-separated nanoparticles. Even when the dispersed state is thermodynamically stable, it may be inaccessible unless the correct processing strategy is adopted, which is particularly important for the case of fullerene dispersion into linear polymers.

Polymer phase stability in solution (*1*) or with another polymer (*2*) has been studied for over 50 years and found to be a delicate balance of entropic and enthalpic contributions to the total free energy. For example, it is possible to fractionate a polymer by size with a small change in solvent quality (*3*) and to control miscibility of chemically identical polymers whose only difference is architecture (branching) (*4*). More recently, the phase stability of nanoparticle-polymer blends has attracted intense scrutiny (*5*) and is challenging to predict because of computational difficulty in accessing the relevant length and time scales. Flory theories, density functional theories, and molecular dynamics methods provide essential guidance, although accurate calculations are restricted to two or at most a few nanoparticles in the relevant size regime (*6*, *7*). Despite these difficulties, a vast array of applications are emerging that require nanoparticle dispersion, such as in the use of fullerenes to enhance the efficiency of polymer-based photovoltaic devices (*8*, *9*) and in the control of polymer viscosity using nanoparticles (*10*).

We demonstrate strategies for control of nanoparticle dispersion in linear polymer melts. We start with discussion of processing procedures that enable stable dispersion of fullerenes and then present an experimental characterization of the parameters that control the phase boundary between the dispersed and phase-segregated states of carefully considered nanoparticle-polymer mixtures. Moreover, it has been proven possible to disperse polyethylene nanoparticles in polystyrene despite the fact that linear polyethylene–linear polystyrene is a classic phase-separating blend, which implies that nanoparticle morphology may actually enhance dispersion. This hypothesis is tested by using a system composed of polystyrene nanoparticles dispersed in linear polystyrene, because the monomer-monomer contacts in this system are the same for all of its constituents. An enthalpic mechanism that arises from nanoparticle packing effects operates at the nanoscale and is necessary in order to understand dispersion in this size regime. A Flory theory, which includes this enthalpic contribution as well as chain stretching caused by nanoparticle dispersion and the standard mixing entropy, is used to reconcile the experimental observations and emphasize the importance of the nanoparticle-to-polymer size ratio in controlling nanoparticle dispersion.

First we discuss the dispersion of fullerenes into polystyrene, motivated by earlier work that suggested that fullerene dispersion in polymers (*11*) is poor, limiting their utility, for example, in solar cells (*8*, *9*). For a polymer blend, the insertion energy of a linear polymer chain with another controls dispersion and grows with the number of monomers in the chain. So, the insertion enthalpy of a chain of N monomers is proportional to $N\chi$, where χ is the Flory mixing parameter and is the primary cause of phase separation in incompatible blends. Nanoparticles have an insertion enthalpy that grows in proportion to the surface area of the nanoparticle, yielding an insertion enthalpy of $s \sim A\chi$, where $A = 4\pi a^2$ for a nanoparticle of radius a. Although this enhancement is not as strong as for polymer blends, dispersion of nanoparticles still depends critically on χ. We observed experimentally that it is possible to disperse up to a concentration of 2 volume % of C_{60} in linear, monodisperse polystyrene. At small nanoparticle concentration, Flory theory (*1*) gives a binodal or phase stability volume frac-

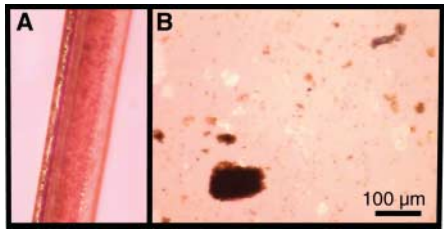

Fig. 1. (**A**) Rapid precipitation of fullerene-polystyrene blends, followed by drying and melt processing, allows manufacture of fibers. The fibers contains 1 wt % C_{60} fullerenes that were melt spun into long fibers with a diameter of circa 1 mm. (**B**) Fullerene (1 wt %)-polystyrene blends developed through regular solvent evaporation produce large, phase-separated domains, which are not apparent in the fiber.

[1]Department of Chemical Engineering and Materials Science, [2]Department of Physics and Astronomy, Michigan State University, East Lansing, MI 48824, USA. [3]Materials Research Laboratory, University of California, Santa Barbara, CA 93106, USA. [4]IBM Almaden Research Center, 650 Harry Road, San Jose, CA 95120, USA. [5]Department of Chemistry, University of California, Irvine, CA 92697, USA.

*To whom correspondence should be addressed. E-mail: mackay@msu.edu